Magnetic order and moment stability in YMn_2

1991 J. Phys.: Condens. Matter 3 6473

(http://iopscience.iop.org/0953-8984/3/33/023)

J. Phys.: Condens. Matter 3 (1991) 6473–6488. Printed in the UK

Magnetic order and moment stability in YMn_2

R Cywinski†, S H Kilcoyne† and C A Scott‡

†J J Thomson Physical Laboratory, University of Reading, Reading RG6 2AF, UK
‡Rutherford Appleton Laboratory, Chilton, Didcot, Oxon OX11 0QX, UK

Received 18 April 1991

Abstract. High-resolution neutron powder diffraction and transverse field μSR measurements have been used to examine the nature of the magnetic and structural transition at 100 K in YMn_2. The neutron measurements indicate a first-order hysteretic transition occurring at 92.5 K on cooling and 108 K on warming. The low-temperature phase is tetragonal ($c/a = 0.995$) and antiferromagnetic with localized Mn moments of 2.8 μ_B ordering in a long-wavelength helix characterized by an antiferromagnetic translation vector $(\tau, \tau', 1)$ where $\tau = 0.018$ and $\tau' = 0.003$. The high-temperature phase is cubic and Pauli paramagnetic. The collapse of the Mn moment at the transition is accompanied by a 5% decrease in the cell volume. In the paramagnetic state of YMn_2 measurement of the muon transverse relaxation rate reveals an underlying second-order transition which we associate with the critical slowing of longitudinal spin fluctuations as the transition temperature is approached.

1. Introduction

YMn_2 is a remarkable C15 Laves phase compound which exhibits a transition from predominantly local moment behaviour at low-temperatures to weak itinerant electron magnetism above 100 K. As a model system through which the mechanisms of moment stabilization can be probed YMn_2 has recently become the focus of extensive and intensive theoretical and experimental effort.

For many years YMn_2 was considered to be a Pauli paramagnet [1]. Indeed susceptibility measurements indicate the absence of localized magnetic moments at temperatures above approximately 100 K [2]. However, neutron diffraction studies [3] reveal that below this temperature there is a first-order transition to an antiferromagnetic state in which a moment of approximately 2.7 μ_B is localized at each Mn site. On cooling the magnetic transition occurs at approximately 70 K and is accompanied by a spontaneous increase of 5% in the volume of the unit cell. On warming, the collapse of the antiferromagnetic structure and the cell volume once again coincide but at a temperature of approximately 120 K. The low-temperature antiferromagnetic structure is itself of great interest: as the Mn sites have tetrahedral topology, and nearest-neighbour Mn–Mn interactions predominate it has been suggested that simple antiferromagnetic structures are frustrated leading to the stabilization of a long period (400 Å) helical ordering of the spins [4].

In contrast to the apparently localized moment behaviour exhibited by its low-temperature ordered phase, above the transition temperature YMn_2 bears all the hallmarks of a weak itinerant antiferromagnet [5–7]: In fact the collapse of the cell

0953-8984/91/336473+16$03.50

volume at T_N is believed to be a consequence of the collapse of the Mn moment itself. Neutron polarization analysis measurements [7] support this view, showing that the amplitude of the Mn moment drops by more than 30% at T_N and then recovers slowly as the temperature increases. These polarization analysis measurements also show strong antiferromagnetic correlations persisting to at least 6 T_N. The persistence of such correlations together with the temperature dependence of the Mn moment are in qualitative agreement with Moriya's theories of spin fluctuations and weak itinerant antiferromagnetism [8, 9]. However, this interpretation is not without controversy: Similar neutron results have been used as evidence for short-range order of Mn moments above T_N, the observed increase in scattering intensity being thought to arise from a reduction of the topological frustration with increasing temperature [10]. This explanation does not appear to be consistent with, for example, NMR [6] or magnetovolume measurements [5]. The latter show an anomalously high thermal expansion coefficient (50×10^{-6}/K) above T_N, in accord with phenomenological spin fluctuation theory [5, 11], and thus lend further support to the itinerant electron model.

It is clear that the characterization of the stability and nature of the Mn moment is essential if the crossover from low-temperature localized moment antiferromagnetism to the high-temperature spin fluctuating state of YMn_2 is to be understood. Such characterization is the aim of the present investigation of the structural and magnetic transitions in YMn_2 in which we use high-resolution neutron powder diffraction to determine the details of the magnetic and structural order above and below T_N, and transverse field muon spin rotation ($^+\mu$SR) techniques to probe the dynamics of the local internal fields as the critical temperature is approached from above.

2. Sample preparation

A 15 g sample of YMn_2 was prepared by argon arc melting appropriate quantities of constituent metals of purity better than 99.9%. An extra 5 at% of Y over the stoichiometric amount was added in order to suppress formation of the strongly ferromagnetic Y_6Mn_{23} compound. After melting, the sample was annealed in an argon atmosphere for 5 days at 800 °C. The resulting material was then crushed to a coarse powder and subjected to a further 5 days at 800 °C in argon.

The same sample was used for the high resolution pulsed neutron powder diffraction and the muon spin rotation measurements both of which were performed at the ISIS facility at the Rutherford Appleton Laboratory.

3. Neutron powder diffraction

The diffraction experiments were carried out on the HRPD diffractometer, a pulsed neutron instrument optimized for high-resolution powder measurements ($\Delta d/d = 5 \times 10^{-4}$) [12]. Briefly, this resolution is achieved by means of a long (100 m) initial flight path for the neutrons, thus reducing the relative uncertainty in the neutron time-of-flight, and by collecting the neutron diffraction patterns in backscattering geometry, for which geometrical contributions to the resolution are minimized. Spectra were collected from a powdered sample of YMn_2 mounted in a vanadium can with planar geometry (25 mm × 15 mm × 3 mm) over the temperature range 4.2 to 160 K covering times-of-flight from 30 to 280 ms, corresponding to a d-spacing range of 0.6 to 5.5 Å.

3.1. Nuclear structure

The powder diffraction patterns obtained from the YMn_2 sample at 160 and 4.2 K are shown in figures 1(*a*) and 1(*b*) respectively. At the higher temperature all the major lines can be indexed as arising from a cubic lattice with space group $Fd\bar{3}m$ and a lattice parameter of 7.6244(6) Å. Rietveld profile refinement of the data confirmed that there is no detectable disorder between the Y atoms at the $(\frac{1}{8}, \frac{1}{8}, \frac{1}{8})$ (8*a*) site and the Mn atoms at the $(\frac{1}{2}, \frac{1}{2}, \frac{1}{2})$ (16*d*) site.

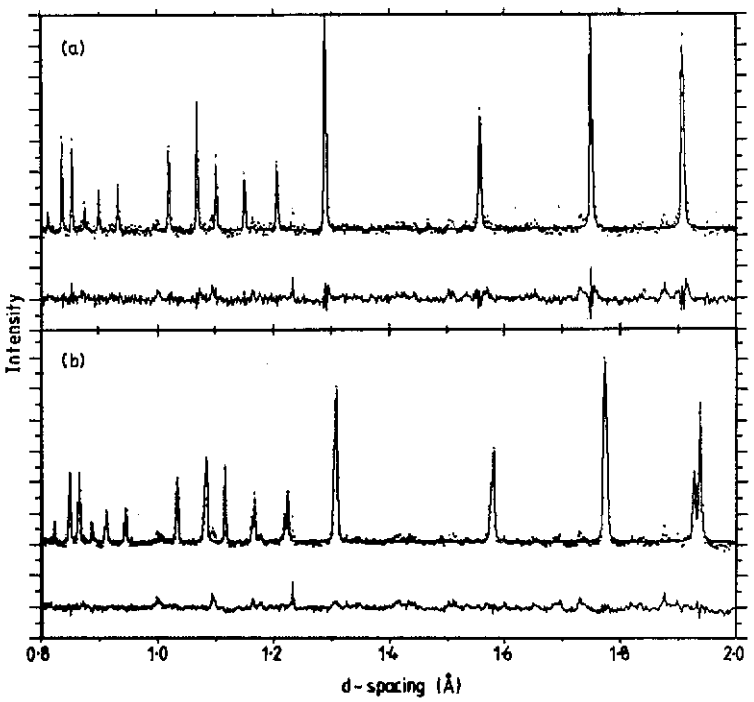

Figure 1. Sections of the YMn_2 powder diffraction patterns collected at (*a*) 160 and (*b*) 4.2 K, shown together with the calculated profiles refined using the Rietveld method with (*a*) the cubic $Fd\bar{3}m$ space group and (*b*) the tetragonal $F4_1/d12/m$ ($14_1/amd$) space group. The differences between the measured and calculated spectra are also shown.

Cooling the sample to 4.2 K results in a number of marked changes in the powder spectrum:

(i) There is a pronounced shift of the Bragg peaks to higher *d*-spacings consistent with a large increase in the dimensions of the unit cell.

(ii) Several of the Bragg peaks show a clear splitting indicative of a change of crystal symmetry.

(iii) New Bragg peaks appear in the spectrum at *d*-spacings commensurate with the magnetic structure reported in references [3, 4, 7].

Points (i) and (ii) are illustrated in figure 2, where the evolution of the powder diffraction pattern in the vicinity of the (4, 0, 0) peak is shown as the sample cools from 160 to 4.2 K.

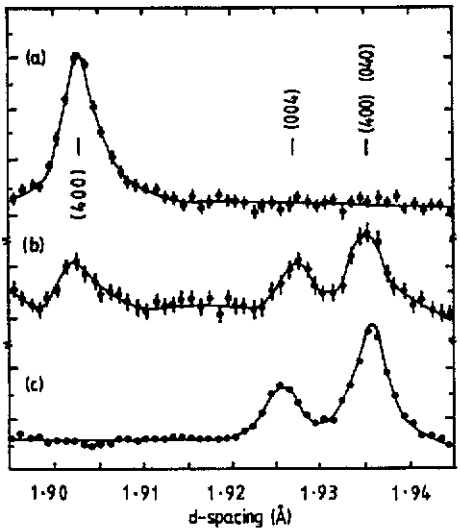

Figure 2. Evolution of the powder diffraction of YMn_2 in the region of the (4,0,0) Bragg reflection on cooling. The data shown were collected at (a) 160, (b) 75 and (c) 4.2 K.

There has previously been some debate over the crystal symmetry of the expanded low-temperature phase of YMn_2. While most authors assume that the lattice remains cubic at all temperatures, it has been suggested that the volume expansion is accompanied by a rhombohedral distortion ($Fd\bar{3}m$ to $F1\bar{3}2/m$ ($R\bar{3}m$)) [13] and alternatively by a tetragonal distortion ($Fd\bar{3}m$ to $F4_1/d12/m$ ($I4_1/amd$)) with $(1-c/a) = 2.3 \times 10^{-3}$ [14]. There is clear evidence for cubic to rhombohedral distortions associated with the onset of magnetic order in other Laves phase compounds (e.g. $Ce(Fe_{1-x}Co_x)_2$ [15]). Such a distortion results in a splitting of Bragg reflections of the type (h,h,h). The diffraction pattern obtained from YMn_2 at 4.2 K, however, shows that only Bragg peaks of the type (h,h,l) and (h,k,l) are split. This result is fully consistent with a tetragonal distortion of the lattice. Rietveld refinement of the 4.2 K spectrum, using the $F4_1/d12/m$ space group, yields the lattice parameters $a = 7.74002(7)$ Å and $c = 7.70009(13)$ Å. The tetragonal distortion is therefore characterized by a magnetostrictive strain of $e = (1-c/a) = 5 \times 10^{-3}$, somewhat larger than that reported in [14]. The total change in cell volume between the high- and low-temperature phases amounts to 4.8%. Detailed results of the Rietveld refinement of the 4.2 and 160 K data are presented in table 1.

Table 1. Structural parameters obtained from Rietveld refinement of HRPD spectra collected from YMn_2 at 4.2 and 160 K.

		Temperature	4.2 K				160 K			
		Space group	$F4_1/d12/m$				$Fd\bar{3}m$			
Atom	Site		x	y	z	B	x	y	z	B
Y	8*a*		0.125	0.125	0.125	0.56	0.125	0.125	0.125	0.81
Mn	16*d*		0.500	0.500	0.500	0.60	0.500	0.500	0.500	0.77
		a (Å)	7.74002(7)				7.62440(6)			
		c (Å)	7.70009(13)				—			
		χ^2	1.35				1.20			

Several diffraction patterns were collected both on cooling from 160 to 4.2 K and again on warming to 160 K. The results obtained from these scans are summarized in figures 3 and 4. Figure 3 shows the variation of the lattice parameters with temperature. It can be seen that above the transition temperature the thermal coefficient of expansion is anomalously large. A value of 48.5×10^{-6}/K is obtained, in close agreement with previous estimates [5]. Figure 4 shows the temperature dependence of the volume fractions of the sample in the high-temperature phase and low-temperature expanded phase, as determined by the relative intensities of the Bragg peaks associated with the two phases. From figure 4 it is clear that the first-order structural transition is hysteretic. On cooling the transition begins at a temperature of approximately 92.5 K, while on warming the unit cell starts to contract rapidly at approximately 108 K. The midpoints of the transitions on cooling and warming are at 80 and 115 K respectively.

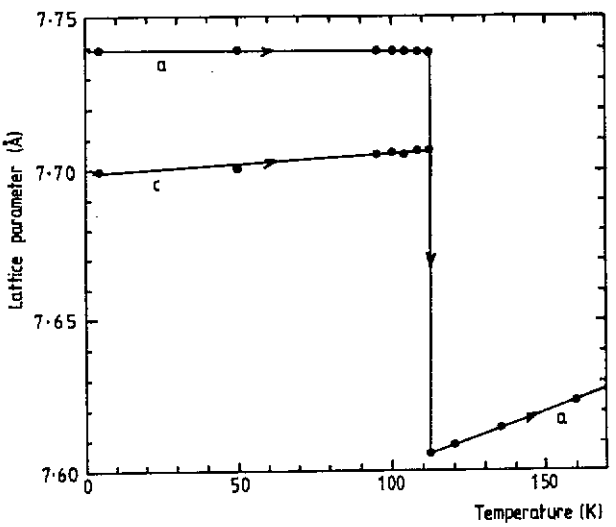

Figure 3. Variation of the lattice parameters of YMn_2 as a function of temperature (on warming).

3.2. Magnetic structure

Detailed analysis of the antiferromagnetic structure observed at low-temperatures is somewhat hampered by the relatively low neutron count rate available on HRPD at appropriately large d-spacings. However, magnetic contributions to the low-temperature spectra collected from the YMn_2 sample are observed at reciprocal lattice points given by $k + l = 2n + 1$. This is characteristic of a type 1 face-centred cubic antiferromagnetic structure with a propagation vector of $(0, 0, 1)$ as previously determined by low-resolution powder diffraction measurements [3, 7] and illustrated in figure 5.

The intensity of a magnetic Bragg reflection measured using a time-of-flight powder diffractometer, such as HRPD, is given by (see e.g. [16])

$$I_{hkl} = G(\theta)i(\lambda)\lambda^4 j_{hkl} q_{hkl}^2 |F_{hkl}^m|^2 f^2(k)$$

where j_{hkl} and F_{hkl}^m are the multiplicity and magnetic structure factor of the reflection (h, k, l). The orientation factor q_{hkl} is determined by the angle between the scattering

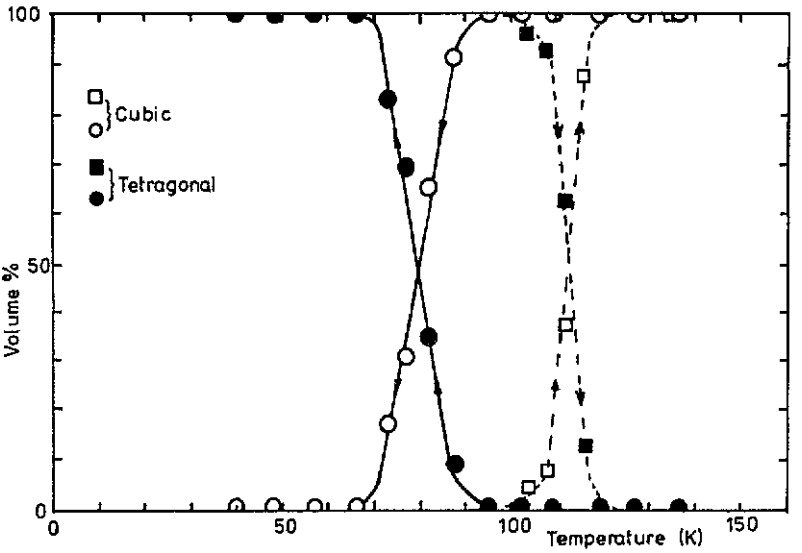

Figure 4. Temperature dependence of the volume fractions of the YMn_2 sample in the high-temperature cubic phase (○, □) and the low-temperature tetragonal expanded phase (●, ■) on cooling (circles) and on warming (squares).

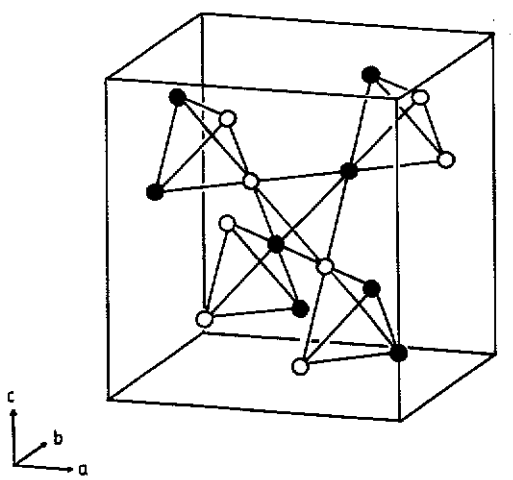

Figure 5. The simple collinear antiferromagnetic structure proposed for YMn_2 [3, 7], ○ represents up-spin and ● down-spin. In the collinear model the spins are oriented at 55° to the c-axis. (Y atoms have been omitted for clarity). The tetrahedral topology of the Mn sites can be clearly seen. In the final, helical, antiferromagnetic model determined here, the Mn spins lay in the (1,0,0) plane but rotate with a period of 430 Å along the a-axis, and a period of 2500 Å along the b-axis.

vector k and the magnetic spin direction, and $f(k)$ is the magnetic form factor (in this case of the Mn^{2+} ion) at a scattering vector of $k = (4\pi \sin\theta)/\lambda$ where 2θ is the scattering angle. $i(\lambda)$ represents the intensity distribution of neutrons of wavelength λ (for the magnetic Bragg peaks considered here $i(\lambda)$ is approximately proportional to λ^{-5}). $G(\theta)$ is a geometrical term.

The *total integrated* magnetic Bragg intensities measured around the (2, 0, 1),

(1, 1, 2) and (3, 1, 0) positions are fully consistent with the simple collinear magnetic structure shown in figure 5 and reported in [3, 7], in which it is assumed that the Mn spins are oriented at 55° to the *c*-axis. A magnetic moment of $2.80 \pm 0.05\ \mu_B$ per Mn atom is determined using the earlier expression. The magnitude of the Mn moment is found to decrease by less than 3% between 4.2 K and the Néel point. However, the antiferromagnetic structure of YMn_2 exhibits a complexity not permitted by this simple model: a distribution of magnetic satellites is observed at each allowed magnetic Bragg position. Ballou *et al* [4] report a similar, though only partially resolved, splitting of the magnetic Bragg peaks and have interpreted this splitting in terms of a modification to the collinear model wherein the modified propagation vector is $(\tau, 0, 1)$ with $\tau = 0.02$. This corresponds to a helimagnetic ordering of Mn spins: the magnetic moments on the Mn atoms in a tetrahedron layer remain collinear within the (1, 0, 0) plane, but moments in adjacent tetrahedral layers, stacked along the [1, 0, 0] direction are rotated through approximately 3.5°.

Following the formalism of Cox *et al* [17], wherein the orientation factor q^2_{hkl} for an antiferromagnetic spiral is given by

$$q^2_{hkl} = \tfrac{1}{4}(1 + \cos^2 \eta_{hkl})$$

with η_{hkl} the angle between the scattering vector for the *hkl* reflection and the normal to the spin plane, we have calculated the intensities of the magnetic satellites according to the model of the magnetic structure described by Ballou *et al* . While this model appears to explain the low-resolution powder diffraction data, it is clearly inadequate for the HRPD data presented here. This can be seen in figure 6 where the calculated intensities and positions of magnetic satellites are shown together with the magnetic Bragg peaks observed in the 4.2 K spectrum. To account for the measured distribution of magnetic satellites we have found it necessary to introduce a further modification to the antiferromagnetic structure. The best fit to the data is obtained with the propagation vector $(\tau, \tau', 1)$ with $\tau = 0.018$ and $\tau' = 0.003$, with the Mn spins lying in the (1, 0, 0) plane. In other words the antiferromagnetic structure of YMn_2 must now be described in terms of two helical components, with the Mn spins rotating in the [1, 0, 0] direction with a period of 430 Å and in the [0, 1, 0] direction with a period of 2500 Å. The final fit of this model for the magnetic structure, with a moment of 2.8 μ_B per Mn atom, is shown by the full line in figure 6.

In fitting both the nuclear and magnetic Bragg peaks it has been necessary to convolute a Lorentzian broadening term with the line shape usually observed on HRPD and described by the Ikeda–Carpenter function [18]. This implies either a particle size broadening effect or intrinsic strain broadening. Analysing the line shape in terms of the former leads to an average particle, or grain, size of approximately 500 Å, i.e. comparable with the wavelength of the magnetic helix. It seems more likely, therefore, that the effect is due to strain within the particles. The half-width of the magnetic Bragg reflections is a little larger than that of neighbouring nuclear Bragg peaks and this may reflect an effective 'strain' within the helix resulting from a clustering of Mn moments along certain easy directions, such as that invoked to account for the results of NMR measurements on YMn_2 at low-temperatures [4].

Ballou *et al* [4] suggest that the helical ordering of the Mn moments is a direct consequence of the topological frustration introduced by the superposition of the simple collinear antiferromagnetic model shown in figure 5 upon the tetrahedral symmetry of the Mn sites. However, earlier workers were unaware of the tetragonality of the

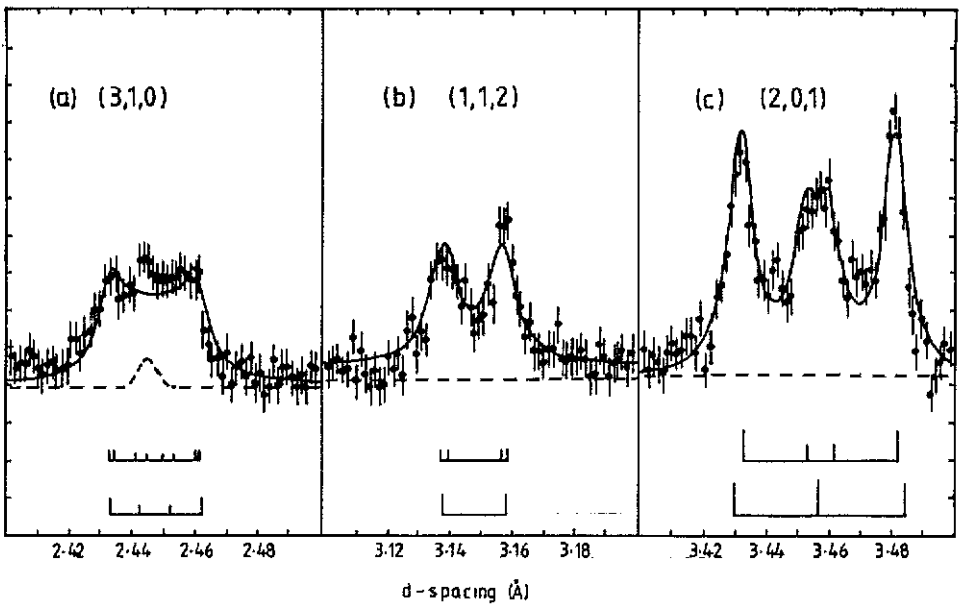

Figure 6. The measured magnetic Bragg scattering around the (*a*) (3,1,0), (*b*) (1,1,2) and (*c*) (2,0,1) positions at 4.2 K. The broken curves represent the 'background' scattering measured above the Néel point at 160 K (note the small impurity peak in (*a*)). The full curves show the fitted profile calculated using our final helical antiferromagnetic structure. Also shown are the positions and relative intensitive of the satellites calculated (i) for this model and (ii) for the model proposed for YMn_2 by Ballou *et al* [4].

low-temperature expanded unit cell. It seems plausible that the massive frustration is more effectively relieved by the tetragonal distortion, confirmed here, rather than by the formation of the long-wavelength helix. (We also note that the magnetic *c*-axis and the tetragonal *c*-axis of the distorted unit cell coincide.)

There remain some interesting questions regarding the nature of the low-temperature antiferromagnetic phase of YMn_2. The helimagnetic model discussed here may well not be a unique solution for the magnetic structure. It is possible (and indeed likely in view of the tetragonal rather than rhombohedral magnetoelastic distortion below T_N [19]) that a multiple-Q structure obtains at low-temperature. Furthermore a spin density wave ground state may adequately explain the observed satellite distribution. A more complete analysis must await further measurements utilizing neutron polarization analysis techniques and single crystal samples, although the possibility of such measurements in conjunction with the uniquely high resolution of HRPD is small.

4. Muon spin relaxation

4.1. The transverse field technique

The positive muon is becoming an increasingly important and popular probe of static and dynamic magnetic spin correlations in metals and alloys (e.g. [20, 21]). The technique involves the implantation of a longitudinally polarized muon in the sample

at time $t = 0$. The muon decays with a time constant τ, of 2.2 μs emitting a positron preferentially in the direction of the muon spin according to the distribution

$$W_\theta = 1 + a_0 \cos\Theta$$

where a_0 is the asymmetry parameter and typically takes the value of 0.25. In the presence of a transverse magnetic flux density B the muon precesses with a Larmor frequency $\omega_L = \gamma B$ where γ is the gyromagnetic ratio of the muon ($\gamma = 8.516 \times 10^8$ rad T^{-1} s^{-1}). With positron detectors positioned in the forward and backward (z)-directions, and the transverse field applied in the x-direction, the measured time-dependent positron count rates are

$$N_{F,B}(t) = N_0 \exp(-t/\tau)[1 \pm a_0 \cos(\omega_L t)] \tag{1}$$

where the + and − signs refer to the forward and backward detectors respectively. Equation (1) assumes that all muons precess with the same frequency. This condition is violated if the muons experience random static local fields, leading to dephasing of the muon precession, or if temporal (transverse or longitudinal) fluctuations of surrounding magnetic dipoles result in fluctuating local fields, producing muon depolarization. In either of these cases we can express the normalized time-dependent count rate as

$$R(t) = \frac{N_F(t) - N_B(t)}{N_F(t) + N_B(t)} = a_0 G_x(t) \cos(\omega_L t). \tag{2}$$

$G_x(t)$ is the transverse relaxation function. In the static limit $G_x(t)$ is Gaussian in form [20]:

$$G_x(t) = \exp(-\sigma^2 t^2) \tag{3}$$

with $\sigma^2 = (\frac{1}{2})\gamma^2\langle B_\mu^2\rangle$, where $\langle B_\mu^2\rangle$ is the second moment of the distribution of flux density at the muon site. On the other hand, if the fluctuation rate, $1/\tau_c$, of the magnetic fields local to the muon site is fast compared with the Larmor frequency, ω, of the muon in the applied transverse field, then exponential relaxation is observed [20]:

$$G_x(t) = \exp(-\lambda t). \tag{4}$$

The Lorentzian damping rate, λ, is given by

$$\lambda = \gamma^2\langle B_\mu^2\rangle\tau_c. \tag{5}$$

4.2. Experimental details

At ISIS the muon beam is pulsed with a repetition rate of 50 Hz. Each pulse consists of two bursts of muons separated in time by 335 ns. In the experiments described here, which employed a conventional transverse geometry, an applied transverse flux density of 22 mT was chosen to minimize the effects of the double pulse structure: the muon precessional rate in this field is such that muons in the first burst and those in the second are exactly in phase after one full precession of the former. The magnitude

of the transverse field is sufficient to decouple the muon from any depolarizing fields arising from static or dynamic nuclear dipoles in the muon environment.

The same YMn_2 sample as used in the neutron powder diffraction measurements was sandwiched between a mylar sheet and an aluminium sample holder, forming a disk 40 mm in diameter by 2 mm thick. This was mounted on the cold stage of a closed cycle refrigerator. The sample temperature could be controlled to within 0.2 K over the range 18–300 K. Measurements were made on cooling the sample to 18 K and on rewarming to 250 K.

The time histograms of the positron count rates observed in the forward and backward detectors at each temperature were grouped according to equation (2), and the resulting $R(t)$ data least-squares fitted using a single exponential relaxation function (Lorentzian damping) indicative of temporal fluctuations in the muons' magnetic environment. Although fits using the Gaussian relaxation function for $G_x(t)$ were possible a significantly higher χ^2 resulted. The addition of a second component, representative of possible background contributions, also led to a poorer fit to the data.

4.3. The muon site in YMn_2

Before discussing the results of the muon measurements it is important to consider the location of the muon within the YMn_2 matrix. In many circumstances the muon behaves like a light isotope of hydrogen. In YMn_2 hydrogen, at low concentrations, is believed to occupy the centre of a tetrahedron surrounded by two Mn and two Y sites, commonly known as the 2–2 site [22]. This is the same site that the muon is thought to occupy in the isostructural RAl_2 Laves phase compounds (R = rare earth) [23]. At higher hydrogen concentrations the 3–1 site, the centre of a tetrahedron composed of three Mn and one Y site, may also be occupied but it is considered unlikely that the muons localize at these sites [23]. At a temperature of 160 K, where the lattice parameter of YMn_2 is 7.6244 Å, the muon–Mn distance is 1.78 Å for the 2–2 site (compared with 1.70 Å for the 3–1 site). A muon at the 2–2 will have a further three next-near-neighbour Mn atoms at a distance of 2.94 Å.

4.4. Results

The results of the data analysis of the muon measurements are summarized in figures 7 and 8. At room temperature the Lorentzian damping rate, λ, is extremely small, typically 0.025 μs^{-1}, indicating a rapidly fluctuating muon environment. The asymmetry term, a_0, is 0.22. On cooling the sample λ begins to increase slowly reaching a value of 0.08 μs^{-1} at 92.5 K at which temperature a_0 decreases rapidly (figure 7). Below 92.5 K λ decreases but reaches a constant value of approximately 0.06 μs^{-1} at 50 K. By this temperature a_0 is also constant at 0.05. The large errors associated with λ below 90 K are a consequence of this small asymmetry.

On warming the sample λ increases reaching a value of 0.075 μs^{-1} at 113 K (figure 8). As can be seen in figure 8(*b*), a_0 remains constant to this temperature then begins to rise again, reaching its original value of 0.22 at 130 K. Above 113 K λ decreases slowly to 0.025 μs^{-1} at 250 K. The temperature dependence of the asymmetry parameter a_0 shown in figures 7(*b*) and 8(*b*) closely mirrors that of the volume fraction of material in the cubic phase of YMn_2, on cooling and warming respectively, as measured by neutron diffraction (figure 4). It can be safely assumed that the rapid decrease of a_0 at low temperatures reflects the onset of long-range antiferromagnetic

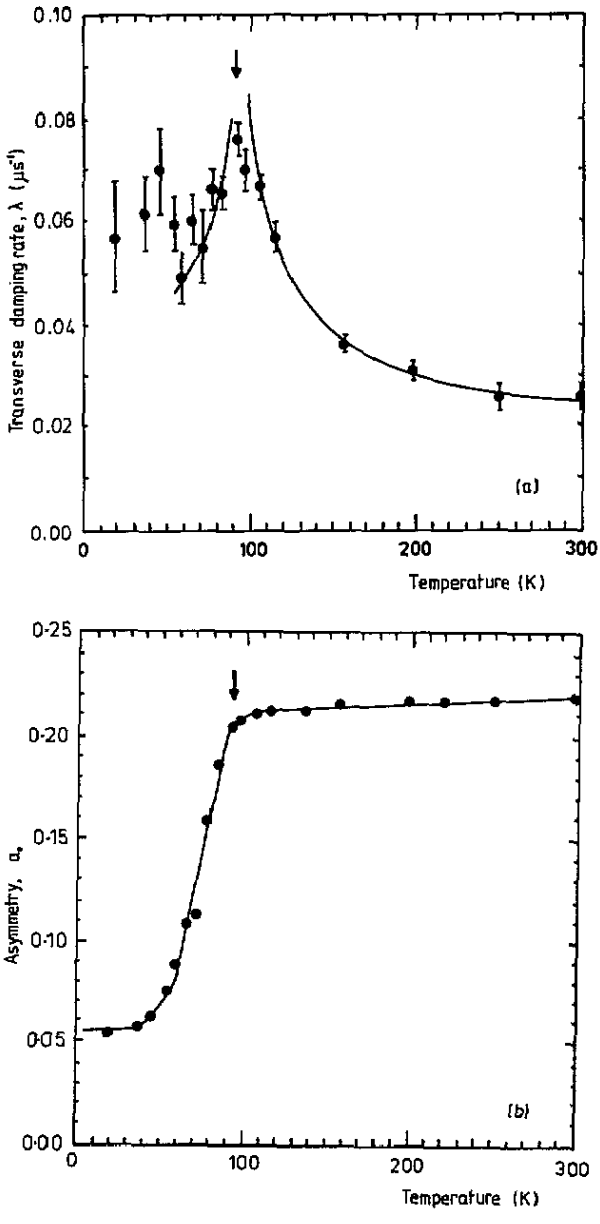

Figure 7. The temperature dependence of (*a*) the transverse Lorentzian damping rate, λ and (*b*) the asymmetry parameter, a_0, obtained from μSR measurements on YMn_2 while cooling. In (*a*) the full curve is a fit of equation (6) to the data, while in (*b*) the curve is a guide to the eye. The arrows in (*a*) and (*b*) represent the temperature at which the first-order structural transition commences as determined by the neutron powder diffraction measurements on cooling.

order in the YMn_2 matrix: the majority of muons occupying sites in the antiferromagnetic expanded phase either see a strong internal field and field distribution which gives rise to a precessional frequency beyond the range of observation available in the present measurements (i.e. $\omega_L > 3 \times 10^7$ rad s^{-1}) or experience a large root-mean-

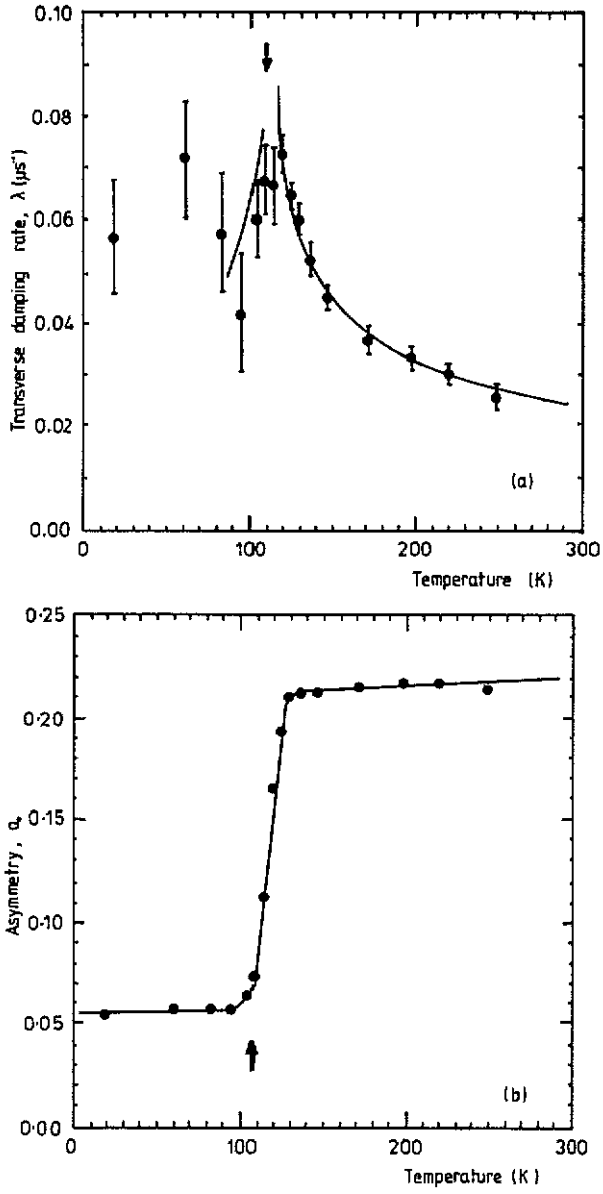

Figure 8. As for figures 7(*a*) and 7(*b*) except the measurements have been made with YMn_2 sample on warming.

square field resulting in a damping rate much faster than that accessible on the ISIS muon facility ($> 5\ \mu s^{-1}$). These muons are therefore effectively removed from the measurement. The reason for the small residual asymmetry at low-temperatures is not entirely clear. It may imply that there remains a small proportion of the muon sites at which the local mean field is close to zero in the antiferromagnetic state.

It should be noted that at all temperatures the fitted value of the observed precessional frequency of the muons, ω_L, remains constant, within experimental error, at 1.87×10^7 rad s^{-1}, fully consistent with that of muons in the applied external flux density of 22 mT. There is no evidence of a muon Knight shift as T_N is approached

from above. Such a shift is generally expected for systems of localized paramagnetic spins close to the ordering temperature.

The behaviour of a_0 is characteristic of a first-order, hysteretic, transition to an antiferromagnetic state, while the temperature dependence of ω_L suggests the absence of localized moments above T_N. The behaviour of the damping rate is quite remarkable. Not only is λ extremely small, between one and two orders of magnitude lower than that observed for isostructural Laves phase compounds [23, 24], its temperature dependence is characteristic of a second-order transition with an extended critical region. This temperature dependence, both on cooling and on warming, is well described by the expression

$$\lambda(T) = \lambda_0(\epsilon)^{-x} \tag{6}$$

where $\epsilon = |T-T_N|/T_N$. x takes the value 0.35 while $T_N = 92.5$ K and $\lambda_0 = 0.033\ \mu s^{-1}$ on cooling and $T_N = 113$ K and $\lambda_0 = 0.031\ \mu s^{-1}$ on warming. Although we do not suggest that x represents a true critical exponent, it can be seen in figures 7(*a*) and 8(*a*) that (6) provides an excellent parameterization of the data. Moreover the 'critical' temperatures determined by fitting this functional form to the data agree very closely with those observed for the transition to and from the expanded low-temperature phase as measured by neutron powder diffraction.

4.5. Discussion

Recently reported preliminary μSR measurements on the pseudobinary compound $(Y_{0.9}Tb_{0.1})Mn_2$ show behaviour that is qualitatively different to that described here for the *pure* YMn_2 sample [25]. Although the asymmetry parameter exhibits an hysteretic first-order transition it also suggests that above T_N there remains a strongly depolarizing contribution, amounting to some 40% of the weakly damped contribution associated with the paramagnetic phase. This contribution decreases slowly with increasing temperature, finally disappearing at 150 K, and is attributed in [25] to magnetic short-range order. The transverse field damping rate is also considerably larger than the values we have reported here for YMn_2. Partial substitution of Y by Tb is known to simplify the low-temperature magnetic structure leading to simple collinear antiferromagnetism [26]. However, our own low-field AC susceptibility and inelastic neutron scattering measurements on dilute rate earth (Ho, Dy, Tb) substituted YMn_2 [27, 28] indicate far more profound changes to the magnetic properties and spin dynamics with, for example, spin glass behaviour being observed at low-temperatures. Pseudobinary compounds formed as with much as 10% Tb substitution for Y cannot therefore be considered to be truly representative of pure YMn_2.

Behaviour consistent with that reported here for YMn_2 was observed in our transverse field μSR measurements on pseudobinary $Y(Mn_{0.97}Fe_{0.03})_2$ [29]. Fe rapidly destabilizes the localized Mn moment by decreasing the Mn–Mn near-neighbour distance and by 2.5 at%Fe substitution all antiferromagnetic order is lost, the compound reverting to Pauli paramagnetism [30]. The muon measurements show a transverse Lorentzian damping rate similar in magnitude to that observed for pure YMn_2, increasing with decreasing temperature, but now diverging at zero rather than a finite temperature. The asymmetry parameter a_0 deviates slightly from its value of 0.22 only at low-temperatures, and as observed here, there is no muon Knight shift within experimental error.

The muon data we have presented in this paper for pure YMn_2 indicate the first-order magnetic and structural phase transition observed in neutron diffraction measurements is accompanied by an underlying broad second-order transition. In our μSR experiments this transition is observed as a critical divergence of the Lorentzian damping rate, λ. In equation (5) it is seen that λ is directly related to both the mean square field at the muon site, $\langle B_\mu^2 \rangle$, and the relaxation time, τ_c, of this field. The divergence of λ thus indicates that one or both of these parameters are temperature dependent. However, from the μSR data alone it is extremely difficult to assess their relative contributions to the observed temperature dependence of λ, nor is the task any simpler when additional information gained from inelastic neutron scattering experiments on YMn_2 (e.g. [7]) is considered: If we consider that the magnetic flux density at the 2–2 muon site arises predominantly from the magnetic dipoles associated with the two near-neighbour (fluctuating and randomly oriented) atomic Mn moments, of approximately 2 μ_B [7], on the tetrahedron surrounding the muon we calculate a value of 0.66 T for the root-mean-square field (this value increasing to 0.8 T when second near-neighbour sites are considered). Substituting this dipole field into equation (5) we find that the characteristic fluctuation rate of the field is 1×10^{11} Hz at T_N rising to 3×10^{11} Hz at 250 K. However, according to the inelastic neutron scattering measurements reported by Freltoft *et al* [7], the spin fluctuations are characterized by an essentially temperature-independent line width, Γ, of approximately 20 meV. This corresponds to a spin fluctuation rate of 4.8×10^{12} Hz, an order of magnitude greater than $1/\tau_c$ determined from the μSR results. More recent inelastic neutron scattering measurements carried out at a higher energy resolution than that available to Freltoft *et al* have indicated a line width, Γ, close to 10 meV for YMn_2 above T_N [27]. While these recent results provide a fluctuation rate which is a little nearer to $1/\tau_c$ obtained by μSR there is once again little evidence for the pronounced temperature dependence exhibited by $1/\tau_c$ calculated using the assumption of a mean square dipolar field that is constant with temperature. Alternatively, if it is assumed that the muon senses the same spin fluctuation rate as that measured by neutron scattering then an unrealistically large root-mean-square field of 2–3 T must be present at the muon site in the Pauli paramagnetic phase of YMn_2.

This disparity between the muon and neutron results is not entirely unexpected. We note that while neutron scattering measures directly the dynamical *spin correlations* of the sample, μSR probes instead the dynamics of *magnetic fields* at the muon site: In cases such as YMn_2, where pronounced dynamic and spatial spin correlations dominate the paramagnetic state it is clear that the neutron and muon data are not simply related and comparisons should be treated with caution.

In conclusion, therefore, we believe that it is not unreasonable to associate the behaviour of λ with the strongly spatially correlated longitudinal spin fluctuations which characterize the Pauli paramagnetic state of YMn_2, the critical slowing down of these fluctuations being responsible for the gradual increase in τ_c, and therefore in λ, as T_N is approached. Indeed it is significant that the first-order transition associated with the structural change and onset of antiferromagnetism, as observed in both the neutron measurements and in the temperature dependence of the muon asymmetry parameter, does not proceed until the critical temperature, T_N, of the second-order transition in λ is reached, perhaps suggesting that the expansion of the cell volume occurs as the longitudinal spin fluctuation rate reaches a critically low value at which the 3d electrons condense at Mn sites. It must be emphasized that the Lorentzian nature and small magnitude of the transverse damping rate observed in

these measurements are not consistent with a model in which localized but frustrated Mn moments dominate the paramagnetic state, as suggested in [10] and [25].

5. Conclusions

The high-resolution powder diffraction measurements described in this paper have provided a more detailed description of the magnetic and structural order in the low-temperature localized moment state of YMn_2 than has previously been available. We find that cooling through the Néel point of 92.5 K results in a first-order transition from Pauli paramagnet to helical antiferromagnet with a well localized magnetic moment of 2.8 μ_B at each Mn site and an antiferromagnetic propagation vector of $(0.018, 0.003, 1)$. At T_N there is a simultaneous increase in the volume of the unit cell of 4.8% together with a tetragonal distortion characterized by a magnetostrictive strain of $e = (1 - c/a) = 5 \times 10^{-3}$. Our transverse field μSR measurements clearly show that these first-order magnetic and structural transitions are accompanied by an underlying second-order transition, manifest as a divergence of the transverse Lorentzian damping rate, λ. We suggest that this divergence of λ is associated with a critical slowing down of longitudinal spin fluctuations, and that it is precisely this slowing down that drives the dramatic transition from itinerancy to local moment behaviour in YMn_2.

Acknowledgments

It is with great pleasure that we acknowledge the support and assistance of the staff at ISIS, and the technical support of Mr A Perkin of the J J Thomson Physical Laboratory. Discussions with Dr S F J Cox have been extremely valuable. We are grateful for financial support from the SERC's Neutron Beam Research Committee.

References

[1] Buschow K H J and Sherwood R C 1978 *J. Appl. Phys.* **49** 1480
[2] Shiga M, Wads H and Nakamura Y 1983 *J. Magn. Magn. Mater.* **31–4** 119
[3] Nakamura Y, Shiga M and Kawano S 1983 *Physica* B **120** 212
[4] Ballou R, Deportes J, Lemaire R, Nakamura Y and Ouladdiaf B 1987 *J. Magn. Magn. Mater.* **70** 129
[5] Shiga M 1988 *Physica* B **149** 293
[6] Yoshimura K, Takigawa M, Yasuoka H, Shiga M and Nakamura Y 1986 *J. Magn. Magn. Mater.* **54–7** 1075
[7] Freltoft T, Boni P, Shirane G and Motoya K 1988 *Phys. Rev.* B **37** 3454
[8] Moriya T 1985 *Spin Fluctuations in Itinerant Electron Magnetism* (Berlin: Springer)
[9] Moriya T 1979 *J. Magn. Magn. Mater* **14** 1
[10] Deportes J, Ouladdiaf B and Ziebeck K R A 1987 *J. Magn. Magn. Mater.* **70** 14
[11] Shiga M 1981 *J. Phys. Soc. Japan* **50** 2573
[12] David W I F, Akporiaye D E, Ibberson R M and Wilson C C 1988 *RAL Report* RAL-99-103
[13] Tagawa Y, Sakuri J, Komura Y, Wada H and Nakamura Y 1985 *J. Phys. Soc. Japan* **54** 591–7
[14] Gaidukova I Yu, Kelarev V V, Markosyan A S, Menshikov A Z and Pirogov A N 1988 *J. Magn. Magn. Mater.* **72** 357–9
[15] Kennedy S J, Murani A P, Cockcroft J K, Roy S B and Coles B R 1989 *J. Phys.: Condens. Matter* **1** 629–36
[16] Windsor C G 1981 *Pulsed Neutron Scattering* (London: Taylor and Francis)
[17] Cox D E, Takei W J and Shirane G 1963 *J. Phys. Chem. Solids* **24** 405–23

[18] Ikeda S and Carpenter J M 1985 *Nucl. Instrum. Methods* A **235** 553–9
[19] Van Laar B 1965 *Phys. Rev.* A **138** 584–7
[20] Schenck A 1985 *Muon Spin Rotation Spectroscopy* (Bristol: Hilger)
[21] Cox S F J 1987 *J. Phys. C: Solid State Phys.* **20** 3187–319
[22] Fujiwara K 1988 *J. Phys. Soc. Japan* **57** 2133–42
[23] Hartman O, Karlsson E, Wappling R, Chappert J, Yaouanc A, Asch L and Kalvius G M 1986 *J. Phys. F: Met. Phys.* **16** 1593–615
[24] Graham R G, Armitage J G M, Riedi P C, Cox S F J and Scott C A 1989 *Muon Studies in Solid State Physics* (Bristol: IOP) pp 41–4
[25] Asch L, Kalvius G M, Litterst F J, Weber M, Munch K H, Kratzer A, Aggarwal K, Schenck A, Gygax F N, Ballou R, Deportes J and Chappert J 1990 *Hyperfine Interact.* **64** 435–8
[26] Berthier Y, Deportes J, Horvatic M and Rouault P 1988 *J. Physique Coll.* C8 **49** 261–2
[27] Rainford B D, Dakin S and Cywinski R 1991 *ICM'91; J. Magn. Magn. Mater.* submitted
[28] Ritter C, Mondal S, Kilcoyne S H, Cywinski R and Rainford B D 1991 *ICM'91; J. Magn. Magn. Mater.* submitted
[29] Cywinski R, Kilcoyne S H, Cox S F J, Scott C A and Schärpf O 1990 *Hyperfine Interact.* **64** 427–34
[30] Cywinski R, Kilcoyne S H, Ritter C and Rodriguez-Carvajal J in preparation